Krzysztof Skorupski, Jens Hellmers, Wen Feng, Janusz Mroczka, Thomas Wriedt, Lutz Mädler

Influence of sintering necks on the spectral behaviour of ITO clusters using the Discrete Dipole Approximation

Krzysztof Skorupski, Jens Hellmers, Wen Feng, Janusz Mroczka, Thomas Wriedt, Lutz Mädler,
Influence of sintering necks on the spectral behaviour of ITO clusters using the Discrete Dipole Approximation,
Journal of Quantitative Spectroscopy and Radiative Transfer,
Volume 159, 2015, Pages 11-18, ISSN 0022-4073,
https://doi.org/10.1016/j.jqsrt.2015.02.021

Influence of sintering necks on the spectral behaviour of ITO clusters using the Discrete Dipole Approximation

Krzysztof Skorupski [a,*], Jens Hellmers [b], Wen Feng [b], Janusz Mroczka [a], Thomas Wriedt [b], Lutz Mädler [a]

[a] Wroclaw University of Technology, Chair of Electronic and Photonic Metrology, Boleslawa Prusa 53/55, 50-317 Wroclaw, Poland
[b] Foundation Institute of Materials Science (IWT), Department of Production Engineering, University of Bremen, Bremen, Germany

ARTICLE INFO

Article history:
Received 2 December 2014
Received in revised form
18 February 2015
Accepted 19 February 2015
Available online 4 March 2015

Keywords:
Fractal aggregates
Light scattering
DDA
Necking
Sintering

ABSTRACT

In this paper we study the spectral behaviour of indium tin oxide (ITO) nanoparticle clusters using different sinter neck models for the connections between the primary particles. The investigations include light scattering calculations based on the Discrete Dipole Approximation (DDA). The corresponding clusters are generated using the Cluster–Cluster algorithm proposed by Filippov et al. Different sintering neck models led to significantly different spectral features. A spectral neck factor that reveals the thickness of the necks connecting the primary particles with a simple measurement method is introduced.

1. Introduction

Nano-particles of the same kind (material, size, shape) can show different properties depending on their spatial arrangement. Agglomerates of sintered nanoparticles are usually divided into two groups (see e.g. [1]): 'soft agglomerates' characterized by weak van der Waals forces holding the particles together and 'hard agglomerates' where the particles are bound chemically, leading to sintering necks and a different surface-to-volume ratio. Both types of agglomerates can lead to different behaviour for conductivity, appearance, rigidity, etc. – see e.g. Jiang et al. [2]. For designing material properties based on such geometry effects and their subsequent production, the ability to distinguish between soft and hard agglomerates is of great importance.

Here, we use light scattering simulations based on the Discrete Dipole Approximation (DDA) [3] to investigate the spectral behaviour of fractal clusters consisting of indium tin oxide (ITO) nanoparticles. ITO, while transparent in thin layers in the visible wavelength region, works as a metal-like mirror in the infra-red region. We chose this conducting oxide for a preliminary case-study to investigate possibilities for the development of an in situ, non-destructive measurement method to determine the thickness of the necks connecting the primary particles of clusters.

In this work we concentrate on optical effects caused by differently sized sintering necks in clusters of spherical ITO primary particles. Such connections were previously studied e.g. by Hellmers et al. [4] for two silver particles, or by Skorupski et al. [5] for black carbon (BC) aggregates. In this paper we are looking for characteristic spectral features which would allow us to derive a specific parameter to describe the connections between the primary particles of a cluster. Such a technique would be useful for on-line measurements in process control [6].

2. Refractive index of ITO

Indium tin oxide (ITO) is a conducting oxide that appears transparent in the visible wavelength area. We use the Drude model approach (see e.g. [7]) to calculate

* Corresponding author.
E-mail address: krzysztof.skorupski@pwr.edu.pl (K. Skorupski).

the corresponding values for the real and the imaginary part of the refractive index. Here, the data published by Franzen [8] is the base for the calculations. Fig. 1 shows the permittivity, the refractive indices (n,k) and the reflectance of the bulk material [7]. The permittivity values of the bulk material also can be used to identify regions of plasmon resonances [9]. From Fig. 1 it is obvious that a spectral investigation of ITO has to be extended to near infrared wavelengths.

3. Fractal-like aggregates

The easiest way of creating aggregate models is to use equivalent-volume spherical particles. However, such a simplification might result in many light scattering simulation errors [10]. The morphological parameters of aggregates can be described by using the fractal geometry and the following equation [11]:

$$N_p = k_f \left(R_g / r_p\right)^{D_f}, \tag{1}$$

in which r_p is the particle radius, k_f is the fractal prefactor and D_f stands for the fractal dimension, which is the main parameter defining the overall shape of the structure – the larger its value the more compact is the aggregate. It varies from D_f=1 (e.g. a line) to D_f=3 (e.g. a cube) and generally is independent of the aggregate size. The fractal prefactor k_f is the parameter that is responsible for the equality sign in Eq. (1). Its value is dependent on the aggregate generation conditions. The radius of gyration R_g is defined as follows:

$$R_g^2 = \frac{1}{N_p} \sum_{i=1}^{N_p} (\vec{r}_i - \vec{r}_0)^2, \tag{2}$$

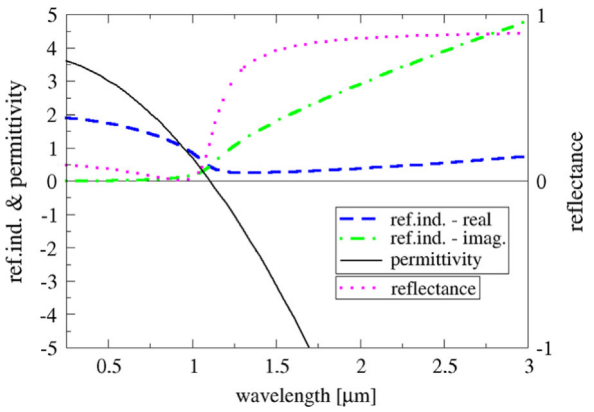

Fig. 1. Permittivity, refractive indices (n,k) and reflectance of bulk material ITO; data by Franzen [8].

where $\vec{r}$ is the position of the ith particle and $\vec{r}_0$ is the mass centre of the aggregate. Eq. (2) is a common approximation widely used in modeling and analysis of fractal-like aggregates [12–15]. It should be noted that there are also different equations, like e.g. by Filippov [16], or by Oh et al. [17], which take into account the radius of gyration of a single sphere. In this work we use Eq. (2) as it has proven to deliver sufficient results, especially as we use monodisperse spheres as primary particles only. For the creation of small aggregates, i.e. composed of N_p=5 primary particles, we used a PC (Particle–Cluster) algorithm and for larger structures we used a CC (Cluster–Cluster) algorithm, which provides more accurate models. Both techniques are based on the work by Filippov et al. [18]. Our implementation reduces the computational time and minimizes the position error that might occur between primary particles. The procedure is described in the work by Skorupski et al. [19]. To characterize fractal aggregates, D_f and k_f are the main parameters for the fractalness of the aggregate. They are independent of the size of the structure. N_p, r_p and R_g are varied as they define the number of primary particles, their radii and their mean distance from the aggregate center. We chose $D_f \approx 1.8$ and $k_f \approx 1.3$ for our work as these are typical values that lead to realistically shaped clusters [11], what is presented in Fig. 2.

To characterize the growing neck between the primary particles of a cluster we used a cylindrical model, which is presented in Fig. 3. It can be visualized as a cylinder with radius r_{con} positioned between the centres of two monodisperse particles with a radius r_p defined as

$$r_{con} = r_p \cdot Y_{con}, \tag{3}$$

Y_{con} stands for the unitless neck size parameter which varies from $Y_{con} = 0$ (no connection) to $Y_{con} = 1$ (full connection). Necks with $Y_{con} < 0.4$ have an almost negligible volume which results in an insufficient number of volume elements (dipoles) for DDA calculations, see Fig. 3. In our work, we kept the total volume of the aggregate, V, constant and the relative volume error lower than $\delta V < 0.05\%$. Therefore, a reduction of the particle radius r_p compensated the growth of the neck Y_{con}. Note that the primary particles never change their position (their centre coordinates are fix), regardless of the neck size parameter Y_{con}. Such an approach models the early stages of the sintering phenomenon [20].

4. Light scattering simulations

In the next part of our study we made sure that the Discrete Dipole Approximation (DDA) [21] method is capable of simulating the light scattered by aggregates

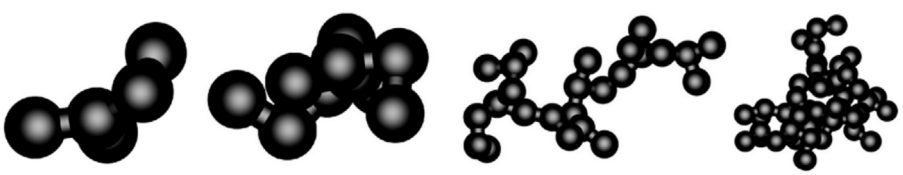

Fig. 2. ITO fractal-like aggregates composed of N_p=5, N_p=10, N_p=25 and N_p=50 primary particles. The neck size parameter is $Y_{con} = 0.5$.

characterized by intermediate and large values of the imaginary part of the complex refractive index, i.e. $k > 1.5$. In our study we decided to use the latest stable version of the ADDA (Amsterdam DDA) [22] algorithm. With its proven reliability and its constant updates it is guaranteed that the resulting simulation error is at its minimum. In a preliminary investigation we compared it to the Nullfield Method with Discrete Sources (NFM-DS), an advanced T-Matrix algorithm by Doicu et al. [23]. A comprehensive description of this method can be found in the monograph by Doicu et al. [24]. NFM-DS has been applied successfully to complex scatterers like elongated fibers [25], flat discs [26], erythrocyte-like shapes [27] and peanut-like shapes [4]. It can also be used to calculate the light scattering behaviour of clusters [12]. To test DDA accuracy, we used already published data for light scattering by peanut-like particles based on Cassini-ovals [4,28]. These curves are characterized in such a way that the product of the distance of two fixed focal points is constant; they are described by the following the Cartesian equation:

$$y = \pm c\left(-a^2 - x^2 \pm \left(4x^2a^2 + b^4\right)^{1/2}\right)^{1/2}. \tag{4}$$

The resulting shape depends on the relation of the two parameters a and b. If $a < b$ the curve is an oval loop, for $a = b$ the result is a lemniscate (like the ∞−symbol) and for $a > b$ the curve consists of two separate loops. For our work we introduce a third parameter c which allows us to manipulate the overall thickness of the shape. The Cassini-oval then is rotated around its longitudinal axis to create the three-dimensional shape describing two sintered spheres, see Fig. 4.

The parameters we chose are $a = 3.07$, $b = 3.50$ and $c = 1.21$, corresponding to a primary particle radius of $r_p = 25$ nm and a resulting total volume of the reference structure of $V_r \approx 130,900\ \text{nm}^3$. For the extinction diagram calculated by the NFM-DS T-Matrix algorithm the results were averaged over 512 ($7 \times 7 \times 7$) orientations [12]. For the ADDA simulations, the reference shape was decomposed into $N_d \approx 130,900$ volume elements (dipoles) with spacing $d = 1$ nm. The solution method was FCDM (Filtered Couple Dipole Method) [21] and the results were orientationally averaged using the Romberg integration in the adaptive regime. The maximum number of orientations was 256 and the integration error was set to 10^{-3} [29]. Both input file types are shown in Fig. 4 and the resulting extinction diagrams are depicted in Fig. 5. One sees that the extreme values for the extinction at $\lambda \approx 1.33\ \mu$m, $\lambda \approx 1.54\ \mu$m and $\lambda \approx 1.79\ \mu$m are less distinct for the ADDA calculations. However, the general curves match well as the extrema occur at the same wavelengths.

The DDA method in general is assumed to give accurate results providing that the distance between volume elements (dipoles) d is much smaller than any characteristic particle dimension. The mesh should be able to precisely describe the shape of the investigated structure. In case when particles are comparable to the wavelength the following rule applies [22]:

$$d = \frac{\lambda}{10|m|}, \tag{5}$$

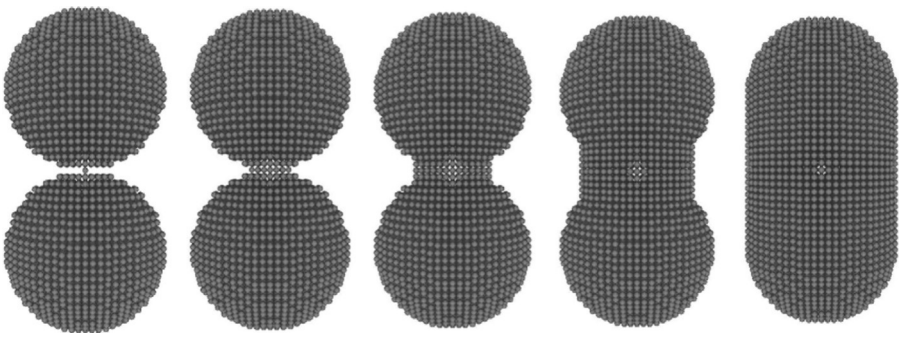

Fig. 3. Assemblies of volume elements (dipoles) required for the DDA simulations. From left to right the value of the neck size parameter varies from $Y_{con} = 0$ to $Y_{con} = 1$ with the step $\Delta Y_{con} = 0.25$. To keep the volume constant the radius of the primary particles slightly shrinks accordingly.

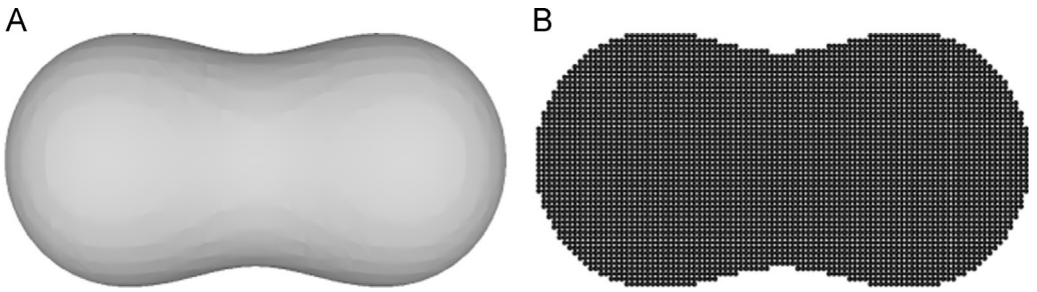

Fig. 4. Two primary particles $N_p = 2$ and a neck based on the rotation of a Cassini oval. Two input files are presented: (A) for the T-matrix simulations and (B) for the ADDA simulations.

where m stands for the complex refractive index, i.e. $m = n + ki$. Another limitations are large computational resources and exceptional simulation time for materials characterized by a large value of the imaginary part of the complex refractive index [21]. For this reason, in our work the wavelength was limited to $\lambda \approx 1.6$ μm.

We analysed whether the previous results can be extended to aggregates composed of more than two particles and investigated the distance between dipoles (volume elements) on a mesh. An exemplary aggregate was composed of $N_p = 50$ particles with radius $r_p = 25$ nm and fractal parameters $D_f = 1.8$, $k_f = 1.3$. To reduce computational time we omitted orientation averaging and concentrated on fixed positions only (the influence of orientation averaging is described in the paragraph at the end of this section). The remaining simulation parameters were left unchanged. Fig. 6 presents the results for $Y_{con} = 0.5$ and $Y_{con} = 1$. For small wavelengths the density of dipoles (volume elements) has only a negligible effect on the extinction coefficient. The discrepancies appear in the plasmon resonance range and diminish with increasing neck size parameter Y_{con}. Once again, the extreme values are underestimated due to the insufficient number of volume elements (dipoles). However, in our work we investigate two reference wavelengths, i.e. $\lambda_1 = 1$ μm and $\lambda_2 = 1.4$ μm (see the following section). The first of them was chosen in the area below the plasmon resonance spectrum and the second one close to the extinction peak.

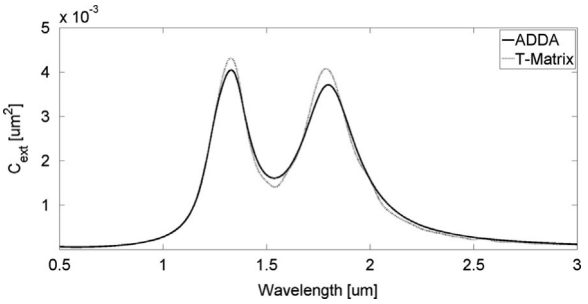

Fig. 5. Comparison of the light scattering results by two different algorithms: T-matrix and DDScat.

The difference in the extinction cross sections C_{ext} at λ_1 was negligible. For λ_2 it was $\Delta C_{ext} = 9.67 \times 10^{-4}$ μm^2 and $\Delta C_{ext} = 6.78 \times 10^{-4}$ μm^2. This resulted in the relative error of $\delta C_{ext} = 1.16\%$ and $\delta C_{ext} = 1.36\%$ for $Y_{con} = 0.5$ and $Y_{con} = 1$ respectively. Finally, we decided to use $d = 1.7$ nm for structures composed of $N_p = 50$ particles, $d = 1.5$ nm for $N_p = 25$, $d = 1.2$ nm for $N_p = 10$, and finally $d = 1$ nm for $N_p = 5$. These settings were based on the estimated accuracy and the simulation time.

Before the extensive simulations of spectra the effects of orientational and configurational averaging were analysed. For the second method we created 256 different geometries characterized by the same morphological parameters. The results for both types of averaging are similar and can be used interchangeably, which is an important finding (Fig. 7): the orientational averaging can be used instead of the configurational averaging, and therefore, we can concentrate on the first type. There is no observable difference between the two curves for $\lambda < 1.2$ μm. Small discrepancies are present at the extinction peak (at $\lambda \approx 1.35$ μm) and at the wavelength of $\lambda = 1.6$ μm where the imaginary part of m becomes more significant. These changes could be caused by a different number of iteration steps (i.e. by using the Romberg integration in the adaptive regime the number of orientations can be lower than 256)

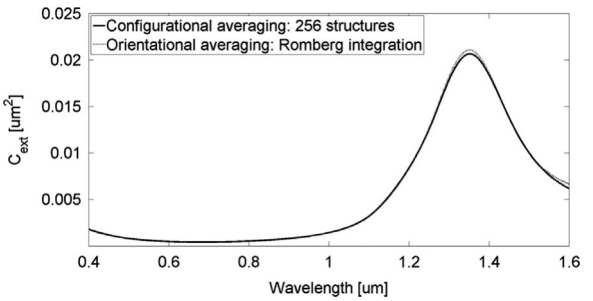

Fig. 7. Comparison between alternative averaging methods: orientational (Romberg integration) and configurational (256 different structures). In our study two reference wavelengths were considered, i.e. $\lambda_1 = 1.0$ μm and $\lambda_2 = 1.4$ μm. At these points, the difference between two curves is barely observable.

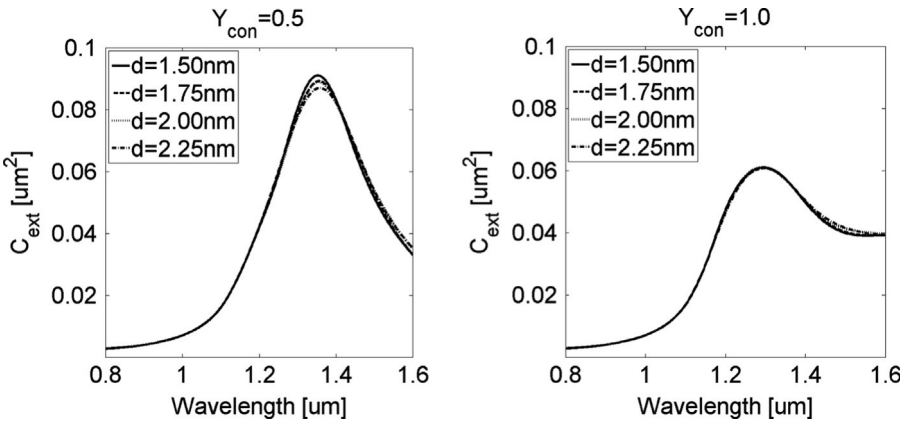

Fig. 6. Impact of the number of volume elements (dipoles) on the extinction diagrams. The simulations were performed for the largest structure in our study, i.e. composed of $N_p = 50$ primary particles. No averaging was performed, i.e. primary particles are in fixed positions.

or by the fact that a single geometry cannot fully recreate the optical properties of a whole set of aggregates.

5. Spectral neck factor (*SNF*)

Our first simulations were performed for $N_p = 10$ connected particles with radius $r_p = 25$ nm. The neck size parameters were $Y_{con} = 0.5$ and $Y_{con} = 1.0$. The ADDA algorithm was used and the distance between volume elements (dipoles) in the resulting mesh was $d = 1.2$ nm. The solution method was FCDM and the results were averaged using the Romberg integration. The extinction diagram is presented in Fig. 8. The difference between the two curves is barely visible when the wavelength is lower than $\lambda < 1.1$ μm. However, the magnitude of the extinction peak as well as its position differ. A closer investigation shows that it is mostly dependent on the absorption cross section C_{abs}, while the effect of the scattering cross section C_{sca} is negligible, see Fig. 9.

For further investigations we selected two separate single wavelengths, here $\lambda_1 = 1$ μm and $\lambda_2 = 1.4$ μm. The first one λ_1 serves as a reference because up to this wavelength there is no observable deviation for different neck sizes. The second wavelength λ_2 is chosen in an area where the influence of the neck size parameter Y_{con} on the extinction is distinct. Its position should not be localized exactly at the wavelength where the extinction peak occurs for the bulk material (compare Fig. 1) because the simulation error associated with the DDA method is at its maximum (see Fig. 6). Therefore, we decided to place λ_2 slightly away from this wavelength but at a point where the difference caused by Y_{con} is clearly observable. The goal is to use these two wavelengths to determine the neck size parameter Y_{con}. We suggest a spectral neck factor that is defined as follows:

$$\mathrm{SNF} = C_{ext}(\lambda_2)/C_{ext}(\lambda_1). \tag{6}$$

The SNF is a largely material dependent parameter. Further investigations for other materials would be necessary to confirm its general adaptability.

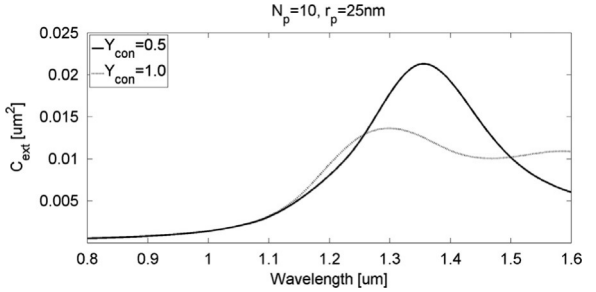

Fig. 8. The extinction cross section C_{ext} of the reference ITO aggregate characterized by two different values of the neck size parameter Y_{con}. The amplitude of the extinction peak is strongly dependent on Y_{con}. The differences in the extinction cross section ΔC_{ext} at the reference wavelengths, i.e. $\lambda_1 = 1.0$ μm and $\lambda_2 = 1.4$ μm, is $\Delta C_{ext} \approx 7.643 \times 10^{-7}$ and $\Delta C_{ext} \approx 8.256 \times 10^{-3}$ respectively.

6. Validation of the results

Results based on one set of morphological parameters only are not a sufficient proof that SNF is a reliable indicator which can be used for the approximation of the neck size parameter Y_{con}. For this reason we created several sets of aggregates characterized by different

Table 1
Morphological parameters of ITO aggregates used in our study. The fractal dimension $D_f = 1.8$ and the fractal prefactor $k_f = 1.3$ are always constant.

N_p	r_p (nm)	d (nm)	D
5	10	0.40	327447
5	25	1.00	327447
5	40	1.60	327447
10	10	0.48	378800
10	25	1.20	378800
10	40	1.92	378800
25	10	0.60	485090
25	25	1.50	485090
25	40	2.40	485090
50	10	–	–
50	25	1.70	666012
50	40	–	–

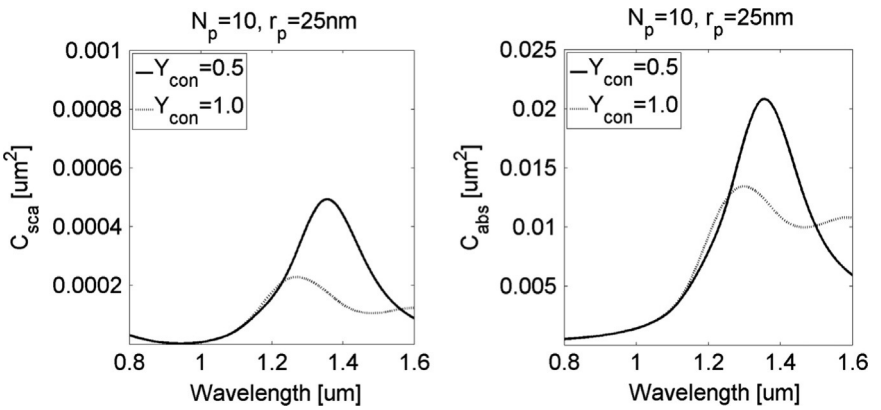

Fig. 9. The the scattering cross section C_{sca} (left) and absorption cross section C_{abs} (right) of the reference ITO aggregate characterized by two different values of the neck size parameter Y_{con}. The extinction cross section C_{ext}, which is defined as $C_{ext} = C_{abs} + C_{sca}$, depends more on the absorption properties of the structure. Note, that the order of magnitude in both figures differs.

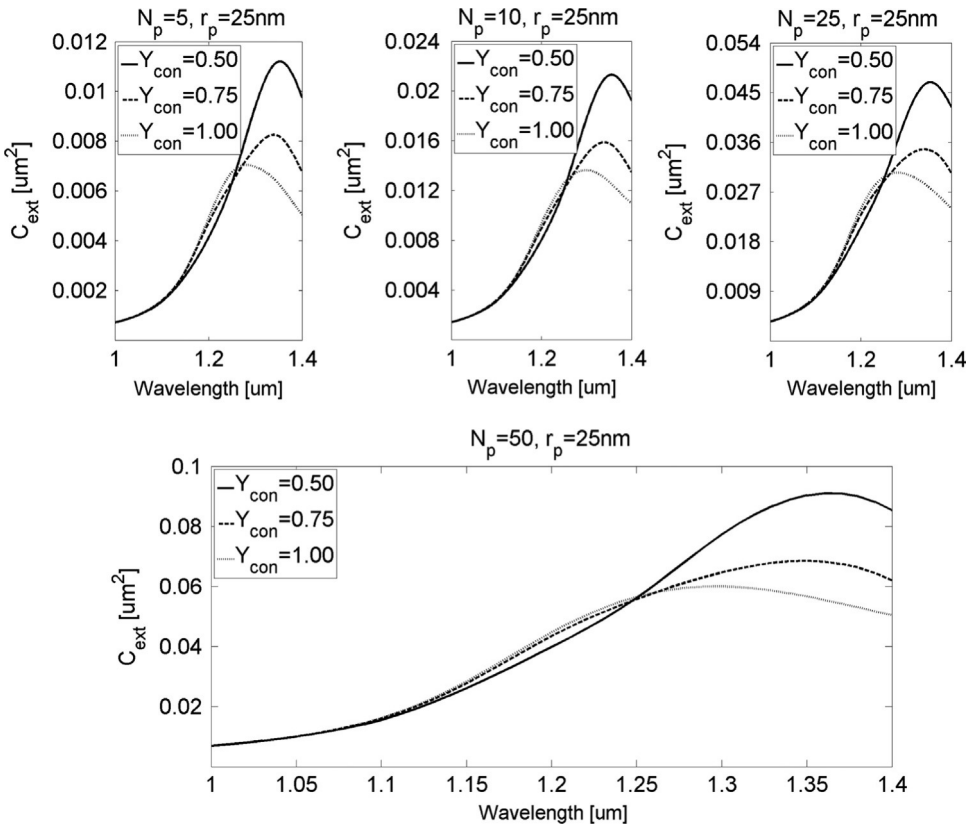

Fig. 10. The extinction cross section C_{ext} as a function of the wavelength λ for three values of the neck size parameter Y_{con} and different numbers of primary particles N_p.

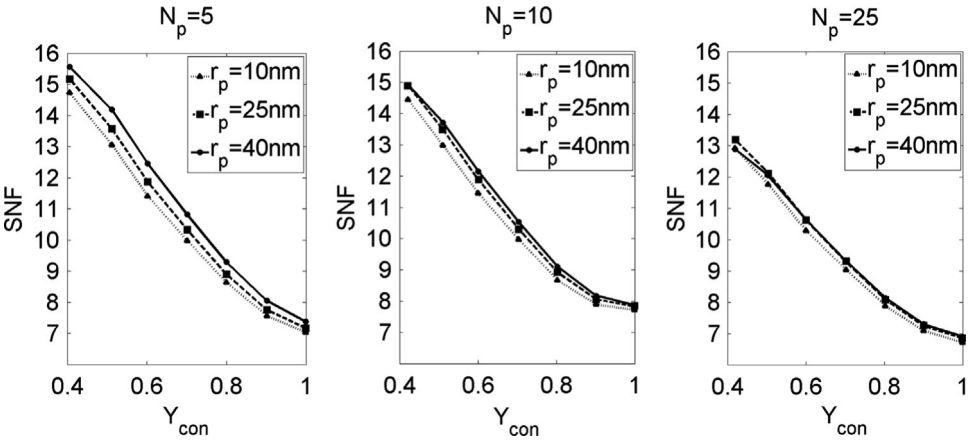

Fig. 11. The SNF (spectral neck factor) as a function of the neck size parameter Y_{con}.

numbers of primary particles N_p and particle radii r_p (Table 1). The total number of volume elements (dipoles) D was dependent on the number of primary particles N_p in ITO structures only, and therefore, the distance d between them is different, i.e. the number of volume elements (dipoles) D for a selected number of particles N_p remains constant, regardless of their radius r_p. The fractal dimension D_f=1.8 and the fractal prefactor k_f=1.3 are constant.

The extinction cross section C_{ext} as a function of the incident wavelength λ is presented in Fig. 10. The results were orientationally averaged. The general shape of the curves is very similar, which shows that the behaviour of the extinction diagrams is independent of the morphological parameters. In every case the extinction peak is suppressed by the growth of interparticle connections. The SNF value decreases gradually for a larger neck size parameter Y_{con}, see Fig. 11.

To verify our findings we did an exemplary comparison to an alternative light scattering algorithm, here SCUFF-EM [30], which is based on the boundary-element method.

The input aggregate consisting of $N_p=25$ primary particles was decomposed into $N_f=5160$ faces for $Y_{con}=0.5$ and $N_f=3264$ faces for $Y_{con}=1$. The results were averaged over 125 ($5\times5\times5$) orientations and are compared in Table 2. Considering that ADDA and SCUFF-EM are based on different scattering theories and that the input geometries for the programs cannot be matched exactly (for ADDA the volume of the cluster is filled up with single dipoles while for SCUFF-EM the surface of the structure is decomposed into triangular patches) the values for SNF are similar. Although the absolute value of SNF might slightly differ if alternative light scattering algorithms are used, the decrease of the extinction peak caused by increased neck size parameter Y_{con} is evident. An extensive comparison between these two scattering theories was not the goal of this paper, and therefore, no study on how to improve the convergence between the results was performed.

The extinction cross section C_{ext} as a function of the incident wavelength λ for $N_p=50$ and $Y_{con}=0.5|0.75|1.0$ is shown in Fig. 10. Table 3 shows the resulting spectral neck factors SNF. The value for $Y_{con}=0.5$ might be lower than expected because DDA underestimates extreme values when the number of volume elements (dipoles) is low (see Fig. 6).

Table 2
Results for the spectral neck factor *SNF* using ADDA and SCUFF-EM.

Scattering code	Y_{con}	*SNF*
ADDA	0.5	12.12
SCUFF-EM	0.5	11.91
ADDA	1.0	6.85
SCUFF-EM	1.0	5.82

Table 3
Results for the spectral neck factor SNF for different neck size parameters Y_{con} for the aggregate composed of $N_p=50$ primary particles.

Y_{con}	0.5	0.75	1.0
SNF	12.25	8.90	7.25

The procedure for retrieving the neck size parameter Y_{con}, e.g. from experimental measurements, is illustrated in Fig. 12. First the SNF is calculated from two distinct wavelengths. Second, the neck size parameter Y_{con} is approximated using a precalculated scattering chart (Fig. 12). It includes all curves for SNF as a function of the neck size parameter Y_{con} for different primary particle radii r_p (comparable to Fig. 11). For example, SNF=10 means that the neck size parameter might vary from $Y_{con}=0.62$ to $Y_{con}=0.75$. If we consider the error caused by the number of volume elements (dipoles), which was approximated previously (see Fig. 6), round it up and assume that its value is δSNF$\approx2\%$ for every Y_{con}, the neck size parameter might vary from $Y_{con}\approx0.61$ to $Y_{con}\approx0.77$. Additionally, because the value of SNF is not totally independent of the number of primary particles N_p a priori information about this parameter could improve the procedure. However, the goal of this paper was to predict Y_{con} for any type of aggregate, and therefore, such a possibility has not been tested.

In our study we assumed that small connections always exist and decided to start with $Y_{con}=0.4$. However, to give a full overview of the investigated phenomenon SNF values for $Y_{con}=0$ are presented in Table 4. Although they are slightly lower than those for $Y_{con}=0.4$ this change is almost negligible. This proves that small connections in ITO clusters cannot be measured with our technique. As

Table 4
SNF values of ITO aggregates used in this study for $Y_{con}=0$, i.e. for particles positioned in point contact.

N_p	r_p (nm)	*SNF*
5	10	14.1302
5	25	14.4807
5	40	14.7679
10	10	14.3778
10	25	14.6758
10	40	14.5050
25	10	12.7389
25	25	12.8964
25	40	12.5138

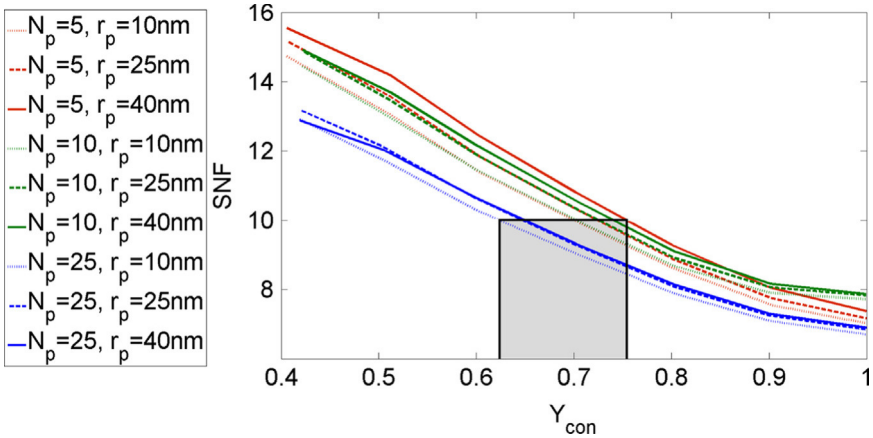

Fig. 12. The procedure for retrieving the neck size parameter Y_{con} from SNF. For example, when SNF=10 the neck size parameter might vary from $Y_{con}\approx0.62$ to $Y_{con}\approx0.75$.

mentioned before, this limitation is caused by the fact that they are almost invisible. The changes of SNF in this regime might be more significant for very small clusters, e.g. composed of $N_p=2$ primary particles, but not for fractal-like aggregates.

7. Summary and conclusions

Our investigation of the impact of the necking phenomenon on the extinction cross section C_{ext} of ITO fractal-like aggregates resulted in an easy and efficient set-up for measuring and/or monitoring the growth of necks between primary particles in ITO aggregates. The extinction peak, positioned at the wavelength of $\lambda \approx 1350$ nm, is strongly influenced by the growth of the neck that exist between each pair of connected particles. This phenomenon is observed regardless of the morphological parameters of ITO aggregates. We propose a procedure for obtaining the neck size parameter Y_{con} with the use of only two reference wavelengths, here $\lambda_1 = 1$ μm and $\lambda_2 = 1.4$ μm, resulting in a spectral neck factor (SNF). Our technique can be used for on-line monitoring of the changes of the morphological parameters of ITO aggregates during the sintering processes.

Acknowledgments

We would like to acknowledge support of this work by Deutsche Forschungsgemeinschaft DFG (GZ: WR 22/43-1).

References

[1] Tsantilis S, Pratsinis S. Soft- and hard-agglomerate aerosols made at high temperatures. Langmuir 2004;20:5933–9.
[2] Jiang H, Moon K, Lu J, Wong C. Conductivity enhancement of nano silver-filled conductive adhesives by particle surface functionalization. J Electron Mater 2005;34(11):1432–9.
[3] Purcell E, Pennypacker C. Scattering and absorption of light by nonspherical dielectric grains. Astrophys J 1973;186:705–14.
[4] Hellmers J, Riefler N, Wriedt T, Eremin YA. Light scattering simulation for the characterization of sintered silver nanoparticles. J Quant Spectrosc Radiat Transfer 2008;109:1363–73.
[5] Skorupski K, Mroczka J. Effect of the necking phenomenon on the optical properties of soot particles. J Quant Spectrosc Radiat Transfer 2014;141:40–8.
[6] Mroczka J. The cognitive process in metrology. Meas: J Int Meas Confeder 2013;46:2896–907.
[7] E. Hecht, Optics, Addison Wesley, San Francisco, 2002.
[8] Franzen S. Surface plasmon polaritons and screened plasma absorption in indium tin oxide compared to silver and gold. J Phys Chem C 2008;112:6027–32.
[9] Cortie M, Giddings J, Dowd A. Optical properties and plasmon resonances of titanium nitride nanostructures. Nanotechnology 2010;21(11):115201.
[10] Li H, Liu C, Bi L, Yang P, Kattawar G. Numerical accuracy of "equivalent" spherical approximations for computing ensemble-averaged scattering properties of fractal soot aggregates. J Quant Spectrosc Radiat Transfer 2010;111:2127–32.
[11] Sorensen CM. Light scattering by fractal aggregates: a review. Aerosol Sci Technol 2001;35:648–87.
[12] Riefler N, Stasio S, Wriedt T. Structural analysis of clusters using configurational and orientational averaging in light scattering analysis. J Quant Spectrosc Radiat Transfer 2004;89:323–42.
[13] Wozniak M, Onofri FRA, Barbosa S, Yon J, Mroczka J. Comparison of methods to derive morphological parameters of multi-fractal samples of particle aggregates from tem images. J Aerosol Sci 2012;47:12–26.
[14] Mroczka J, Wozniak M, Onofri FRA. Algorithms and methods for analysis of the optical structure factor of fractal aggregates. Metrol Meas Syst 2012;19:459–70.
[15] Ringl C, Urbassek HM. A simple algorithm for constructing fractal aggregates with pre-determined fractal dimension. Comput Phys Commun 2013;184:1683–5.
[16] Filippov A. Drag and torque on clusters of n arbitrary spheres at low Reynolds number. J Colloid Interface Sci 2000;229:184–95.
[17] Oh C, Sorensen CM. The effect of overlap between monomers on the determination of fractal cluster morphology. J Colloid Interface Sci 1997;193:17–25.
[18] Filippov A, Zurita M, Rosner D. Fractal-like aggregates: relation between morphology and physical properties. J Colloid Interface Sci 2000;229:261–73.
[19] Skorupski K, Mroczka J, Wriedt T, Riefler N. A fast and accurate implementation of tunable algorithms used for generation of fractal-like aggregate models. Phys A: Stat Mech Appl 2014;404:106–17.
[20] Shimosaka A, Ueda Y, Shirakawa Y, Hidaka J. Sintering mechanism of two spheres forming a homogeneous solid solubility neck. KONA 2003;21:219–33.
[21] Yurkin M, Min M, Hoekstra A. Application of the discrete dipole approximation to very large refractive indices: filtered coupled dipoles revived. Phys Rev E 2010;82:036703.
[22] Yurkin M, Hoekstra A. The discrete dipole approximation: an overview and recent developments. J Quant Spectrosc Radiat Transfer 2007;106:558–89.
[23] Doicu A, Wriedt T. T-matrix method for electromagnetic scattering from scatterers with complex structure. J Quant Spectrosc Radiat Transfer 2001;70:663–73.
[24] Doicu A, Wriedt T, Eremin Y, editors. Light scattering by systems of particles; null-field method with discrete sources: theory and programs. Berlin, Heidelberg: Springer; 2006.
[25] Pulbere S, Wriedt T. Light scattering by cylindrical fibers with high aspect ratio using the null-field method with discrete sources. Part Part Syst Charact 2004;21(3):213–8.
[26] Hellmers J, Wriedt T, Doicu A. Light scattering simulation by oblate discspheres using the null-field method with discrete sources located in the complex plane. J Mod Opt 2006;53:267–82.
[27] Wriedt T, Hellmers J, Eremina E, Schuh R. Light scattering by single erythrocyte: comparison of different methods. J Quant Spectrosc Radiat Transf 2006;100:444–56.
[28] Hellmers J, Wriedt T. Applicability of T-matrix light scattering simulations for the spectral investigation of sintered nanoparticles. J Quant Spectrosc Radiat Transf 2013;123:53–61.
[29] P.J. Davis, P. Rabinowitz. Methods of numerical integration. New York: Academic Press; 1975.
[30] Homer Reid MT, Johnson SG. Efficient computation of power, force, and torque in BEM scattering calculations. ArXiv e-prints ⟨http://homerreid.com/scuff-EM⟩.